electronics

MDPI

Article

Analytical Solutions of the 3-DOF Gyroscope Model

Izabela Krzysztofik * and Slawomir Blasiak

Faculty of Mechatronics and Mechanical Engineering, Kielce University of Technology, Aleja Tysiąclecia Państwa Polskiego 7, 25-314 Kielce, Poland; sblasiak@tu.kielce.pl

* Correspondence: pssik@tu.kielce.pl; Tel.: +48-41-34-24-321

Abstract: The motion of a rigid body (a gyroscope) is one of the key issues in classical mechanics. It remains a significant challenge, as evidenced by its extensive practical implementations in various scientific disciplines and engineering operations. It is important to obtain analytical solutions, as they provide solutions that depend directly on the system's parameters, which can be definitively interpreted. The coupling of numerical and analytical solutions allows for a more precise representation of the real phenomenon. The main objective of the article was to formulate analytical solutions for the motion of a Cardan suspension gyroscope subjected to controlling torque moments. Analytical solutions for the proposed mathematical model were developed using the Laplace transform and Green's function. Subsequently, they were validated by numerical tests. The obtained analytical solutions are universally applicable, regardless of the type of controlling moments.

Keywords: gyroscope; Lagrange's dynamic equations; Green's functions

1. Introduction

The motion of a rigid body (a gyroscope) is one of the key issues in classical mechanics. It remains a significant challenge, as evidenced by its extensive practical implementations in various scientific disciplines and engineering operations [1]. The renowned mathematician L. Euler devised the mathematical principles of the gyroscopic motion theory in the 18th century. Research carried out by eminent scientists such as Lagrange, D'Alambert, and Laplace has contributed greatly to understanding rotating motion. Foucault, the famous French scientist, introduced practical applications of the gyroscope in engineering. He designed a device in which he placed a rapidly rotating axially symmetrical body in a Cardan universal joint. He conducted a series of his laboratory studies and proved the existence of the daily rotation of the Earth. Subsequently, in the 20th century, the advancement of industry and its associated engineering pursuits resulted in the growth of applied gyroscope systems theory. The papers [2,3] investigated gyroscopic effects from the perspective of kinetic energy behavior and through the effect of changing the angular momentum of the rotating rotor.

Nowadays, numerous authors are still tackling the issue of gyroscopic movement. The dynamics of a gyroscope positioned on a vibrating base with linear or non-linear damping, subjected to external disturbances, were the subject of analysis in the papers [4–16]. The effective control of the chaos and synchronization of the chaotic behavior of two gyroscopes required the application of various control methods, including, for instance: delayed feedback control, adaptive control algorithm [4–6], active control [7,8], fuzzy logic control [9,10], variable structure control [11], sliding mode control [12], fuzzy sliding mode control [13], and adaptive fuzzy sliding mode control [14]. The papers [15–17] designed and tested a sliding mode controller and a fuzzy sliding mode controller that shape the movement of a gyroscope from chaotic motion to periodic motion. In turn, in the article [4] the author carried out an in-depth analysis and presented a numerical solution to the issue of symmetric motion of a rigid body in accordance with the Lagrange

check for updates

Citation: Krzysztofik, I.; Blasiak, S. Analytical Solutions of the 3-DOF Gyroscope Model. *Electronics* **2024**, *13*, 1843. https://doi.org/10.3390/electronics13101843

Academic Editors: Olivier Sename and Davide Astolfi

Received: 9 March 2024
Revised: 9 April 2024
Accepted: 7 May 2024
Published: 9 May 2024

case, under the impact of gyroscope vector momentum, perturbing turbine moments, and Newton field.

The modern industry widely uses MEMS (Micro-Electromechanical Systems) and optical gyroscopes as angular velocity sensors. However, mechanical gyroscopes are still used in aeronautics, navigation systems, the engineering industry, as a drive in target coordinators for self-guided missiles, as an executive organ in spacecraft control systems, and in autonomous space exploration systems [18,19]. Mechanical gyroscopes primarily consist of a rotating disc, and an axial shaft as well as frames. The gyroscope rotor set in rotary motion at high speed maintains its original axis of rotation. Only minor processional motions occur. Mechanical gyroscopes are the primary components of navigation devices and control systems due to their ability to maintain the axis of the rotating rotor stable in space. Therefore, in [19] a general model of a controlled gimbal gyroscope on board a flying object (e.g., rocket, UAV) was presented and an algorithm for the optimal correction and stabilization of the gyroscope in the presence of external disturbances was developed and numerically tested. A proposal has been made [20] to use a gyroscope in a scanning–tracking system for searching and observing airborne targets from a moving military vehicle. The authors have designed four types of controllers with MIMO structure: classical PD with optimal parameters, fuzzy PD controller, fuzzy PID controller, and adaptive fuzzy controller. They have numerically verified the controllers. An example of the practical application of the Cardan gyroscope is presented in [21]. The authors proposed a method for dynamically controlling the construction of a tower, which is subjected to wind loads and earthquakes, using multiple Cardan gyroscopes as dampers.

Recent publications [22–24] have concentrated on the techniques and control systems of a gyroscope. The article [22] contains the design of a control structure involving a back-stepping controller, a nonlinear disturbance observer, and two third-order reference models for a double-gimbal control moment gyro subject to extragenic and endogenic distortions, such as frictional resistance moment, coupling moment, and non-modelled dynamics. The systems are subject to various disturbances, such as friction moments, coupling moments, and unmodelled dynamics, both exogenous and endogenous. The study [23] presented control principles that use model predictive control (MPC) for DGSPCMG (a double-gimbal scissored-pair control moment gyro), taking into account gimbal angle restrictions and gimbal velocity limits. The proposed control laws can directly ensure the optimal gimbal control speed with nonlinear real-time constraints, without using the inverse Jacobian matrix of the gyro model. Therefore, when determining the speed of controlling the gimbal of this system, there is no need to consider any peculiarities. In turn, article [24] addresses the issue of preventing singularities in the cluster configuration of four single-gimbal control moment gyroscopes (SGCMG) used for satellite position control. The proposed new SGCMG cluster project has been compared to the VSCMG cluster (variable-speed control moment gyroscopes). The proposed project utilizes an additional stepper motor capable of rotating the entire cluster.

The importance and relevance of the dynamics of motion and gyroscopic control is evident. From a practical perspective, the forces and motion of a gyroscope are expressed using Euler–Lagrange's equations and then solved numerically. The motion equations have been analytically solved only for specific scenarios with significant constraints. The article [18] proposes a certain new analytical approach to gyroscope movements with one side support. The mathematical model was formulated taking into account the effects of load, moments of inertia, and friction. It was subsequently validated through practical tests.

Analytical solutions are significant as they provide solutions that depend directly on the system's parameters, which can be definitively interpreted. The coupling of numerical and analytical solutions allows for a more precise representation of the real phenomenon. The main objective of the article is to formulate analytical solutions for the motion of a Cardan suspension gyroscope subjected to controlling torque moments. Analytical solutions for the proposed mathematical model were developed using the Laplace transform and

Green's function. Subsequently, they were compared to numerical solutions. The analytical solutions obtained are universally applicable, regardless of the type of controlling moments.

This article is organised in the following manner: Section 2 presents a mathematical model of the motion of a gyroscope with a Cardan suspension, along with the analytical solutions obtained. Section 3 contains a comparison of numerical and analytical results. Section 4 presents some conclusions and suggests paths for future research.

2. Subject of Research

The gyroscope shown in Figure 1 was used in the experiment. This is a classic form of a gyroscope. The rotor is an axisymmetric body that rotates around its main axis of symmetry, known as the gyroscopic axis or axis of rapid rotation. The Cardan joint allows for the transverse angular movements of this axis. The quantities used in the figure mean the following: $\omega_x, \omega_y, \omega_z$—components of the angular velocity of the base, θ_w, θ_z—angles of inclination and deviation of the gyroscope axis in space, O, x, y, z—coordinate system associated with the base, O, x_1, y_1, z_1—coordinate system associated with the outer frame, O, x_2, y_2, z_2—coordinate system associated with the inner frame, O, ξ, η, ζ—coordinate system associated with the rotor, and $\vec{U}_w$, $\vec{U}_z$—the vectors of moments of the control forces acting on the inner frame and on the outer frame, respectively.

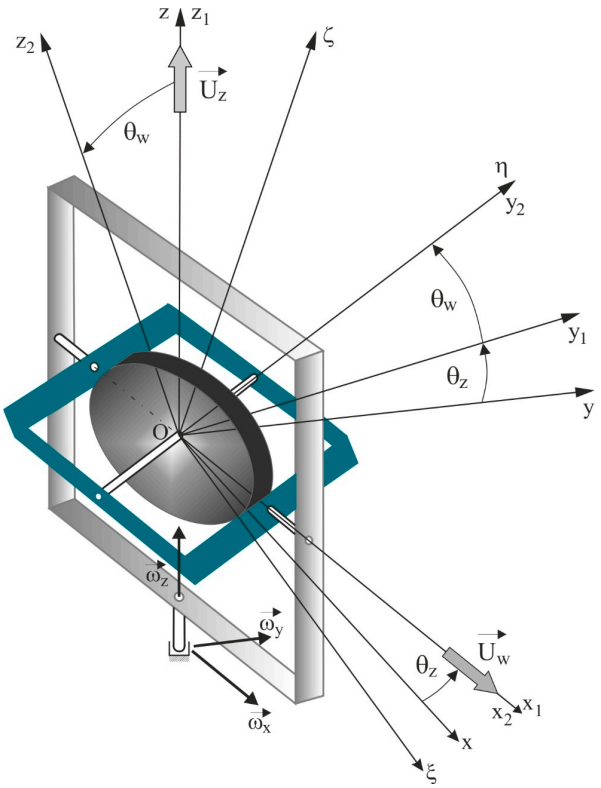

Figure 1. Gyroscope diagram.

The general mathematical model for the motion of a gyroscope on a movable base is presented in the papers [19,20]. It is a system of two strongly nonlinear second-order ordinary differential equations. However, it is often assumed for simplicity that the center of mass of the gyroscope rotor coincides with the center of rotation and the inertia of its frames is neglected. Then, the equations of motion are of the form:

$$\begin{aligned} &J_{rt}\frac{d^2\theta_w}{dt^2} + \eta_w\frac{d\theta_w}{dt} + J_{rt}\frac{d\omega_{x_1}}{dt} - J_{ro}n_o\omega_{y_1}\sin\theta_w + J_{ro}n_o\omega_{z_1}\cos\theta_w + \\ &-\tfrac{1}{2}J_{rt}\omega_{y_1}^2\sin 2\theta_w + \tfrac{1}{2}J_{rt}\omega_{z_1}^2\sin 2\theta + J_{rt}\omega_{y_1}\omega_{z_1}\cos 2\theta_w = U_w \end{aligned} \tag{1}$$

$$\begin{aligned} &J_{rt}\frac{d\omega_{z_1}}{dt}\cos^2\theta_w + \eta_z\frac{d\theta_z}{dt} - \frac{1}{2}J_{rt}\frac{d\omega_{y_1}}{dt}\sin 2\theta_w - J_{rt}\omega_{y_1}\frac{d\theta_w}{dt}\cos 2\theta_w + \\ &-J_{rt}\omega_{z_1}\frac{d\theta_w}{dt}\sin 2\theta_w - J_{ro}n_o\left(\omega_{x_1} + \frac{d\theta_w}{dt}\right)\cos\theta_w - J_{rt}\omega_{y_1}\left(\omega_{x_1} + \frac{d\theta_w}{dt}\right) + \\ &+J_{rt}\omega_{x_1}\omega_{y_1}\sin^2\theta_w - \frac{1}{2}J_{rt}\omega_{x_1}\omega_{z_1}\sin 2\theta_w = U_z \end{aligned} \tag{2}$$

where:

$$\omega_{x_1} = \omega_x\cos\theta_z + \omega_y\sin\theta_z,$$

$$\omega_{y_1} = -\omega_x\sin\theta_z + \omega_y\cos\theta_z,$$

$$\omega_{z_1} = \frac{d\theta_z}{dt} + \omega_z.$$

Furthermore, the angular velocities of the base are equal to zero, and the control moments are functions of time:

$$U_w = f(t) \tag{3}$$

$$U_z = f(t) \tag{4}$$

In this case, the mathematical model of the gyroscope's motion is as follows:

$$J_{rt}\frac{d^2\theta_w}{dt^2} + \eta_w\frac{d\theta_w}{dt} + J_{ro}n_o\frac{d\theta_z}{dt} = U_w \tag{5}$$

$$J_{rt}\frac{d^2\theta_z}{dt^2} + \eta_z\frac{d\theta_z}{dt} - J_{ro}n_o\frac{d\theta_w}{dt} = U_z \tag{6}$$

where:

θ_w, θ_z—angles of inclination and deviation of the gyroscope axis in space;

J_{ro}, J_{rt}—the appropriate moments of inertia in the longitudinal and transverse directions of the gyroscopic rotor;

n_o—rotational speed of the gyroscope;

η_w, η_z—suspension bearing friction coefficients;

U_w, U_z—moments of control forces acting on gyroscope frames.

By applying Laplace's transform to each function (5) and (6) its derivatives, an analytical solution for the system of equations was obtained.

$$\mathcal{L}\{f(t)\} = \overline{f}(s) \tag{7}$$

$$\mathcal{L}\{f'(t)\} = s\mathcal{L}\{f(t)\} - f(0) = s\overline{f}(s) - f(0) \tag{8}$$

$$\mathcal{L}\{f''(t)\} = s^2\mathcal{L}\{f(t)\} - sf(0) - f'(0) = s^2\overline{f}(s) - sf(0) - f'(0) \tag{9}$$

$$\mathcal{L}\{\sin(\omega t)\} = \frac{\omega}{s^2+\omega^2} \tag{10}$$

$$\mathcal{L}\{\cos(\omega t)\} = \frac{s}{s^2+\omega^2} \tag{11}$$

Substitution of the Laplace transformation into Equations (7)–(9) yields:

$$J_{rt}\left(s^2\overline{\theta}_w(s) - s\theta_w(0) - \frac{d\theta_w}{dt}(0)\right) + \eta_w\left(s\overline{\theta}_w(s) - \theta_w(0)\right) + J_{ro}n_o\left(s\overline{\theta}_z(s) - \theta_z(0)\right) = \overline{U}_w(s) \tag{12}$$

$$J_{rt}\left(s^2\overline{\theta}_z(s) - s\theta_z(0) - \frac{d\theta_z}{dt}(0)\right) + \eta_z\left(s\overline{\theta}_z(s) - \theta_z(0)\right) - J_{ro}n_o\left(s\overline{\theta}_w(s) - \theta_w(0)\right) = \overline{U}_z(s) \tag{13}$$

Considering the initial conditions

$$\frac{d\theta_w}{dt}(0) = \theta_w(0) = \frac{d\theta_z}{dt}(0) = \theta_z(0) = 0 \tag{14}$$

The Equations (5) and (6) take into account

$$J_{rt}s^2\overline{\theta}_w(s) + \eta_w s\overline{\theta}_w(s) + J_{ro}n_o s\overline{\theta}_z(s) = \overline{U}_w(s) \tag{15}$$

$$J_{rt}s^2\overline{\theta}_z(s) + \eta_z s\overline{\theta}_z(s) - J_{ro}n_o s\overline{\theta}_w(s) = \overline{U}_z(s) \tag{16}$$

Or after dividing by J_{rt}

$$s^2\overline{\theta}_w(s) + \frac{\eta_w}{J_{rt}}s\overline{\theta}_w(s) + \frac{J_{ro}n_o}{J_{rt}}s\overline{\theta}_z(s) = \frac{1}{J_{rt}}\overline{U}_w(s) \tag{17}$$

$$s^2\overline{\theta}_z(s) + \frac{\eta_z}{J_{rt}}s\overline{\theta}_z(s) - \frac{J_{ro}n_o}{J_{rt}}s\overline{\theta}_w(s) = \frac{1}{J_{rt}}\overline{U}_z(s) \tag{18}$$

Performing a series of analytical calculations and applying the following substitution $a = \frac{1}{2}\left(\frac{\eta_z+\eta_w}{J_{rt}}\right)$, $b^2 = \left(\frac{\eta_w\eta_z+(J_{ro}n_o)^2}{{J_{rt}}^2}\right) - \frac{1}{4}\left(\frac{\eta_z+\eta_w}{J_{rt}}\right)^2 > 0$, $A = \frac{1}{(2a+a^2+b^2)}$, $B = -\frac{1}{(2a+a^2+b^2)}$, $A + B = 0$, $C = 0$, (see Appendix A) the following result was obtained:

$$\begin{aligned}
\overline{\theta}_w(s) = \; & -A\tfrac{J_{ro}n_o}{{J_{rt}}^2}\int_0^t \overline{U}_z(s)\tfrac{1}{s}d\tau + A\tfrac{J_{ro}n_o}{{J_{rt}}^2}\int_0^t \overline{U}_z(s)\tfrac{s+a}{(s+a)^2+b^2}d\tau + \\
& -A\tfrac{J_{ro}n_o}{{J_{rt}}^2}\tfrac{a}{b}\int_0^t \overline{U}_z(s)\tfrac{b}{(s+a)^2+b^2}d\tau + A\tfrac{\eta_z}{{J_{rt}}^2}\int_0^t \overline{U}_w(s)\tfrac{1}{s}d\tau + \\
& -A\tfrac{\eta_z}{{J_{rt}}^2}\int_0^t \overline{U}_w(s)\tfrac{s+a}{(s+a)^2+b^2}d\tau + A\tfrac{\eta_z}{{J_{rt}}^2}\tfrac{a}{b}\int_0^t \overline{U}_w(s)\tfrac{b}{(s+a)^2+b^2}d\tau + \\
& \tfrac{1}{J_{rt}b}\int_0^t \overline{U}_w(s)\tfrac{b}{(s+a)^2+b^2}d\tau
\end{aligned} \tag{19}$$

$$\begin{aligned}
\overline{\theta}_z(s) = \; & A\tfrac{J_{ro}n_o}{{J_{rt}}^2}\int_0^t \overline{U}_w(s)\tfrac{1}{s}d\tau - A\tfrac{J_{ro}n_o}{{J_{rt}}^2}\int_0^t \overline{U}_w(s)\tfrac{s+a}{(s+a)^2+b^2}d\tau + \\
& A\tfrac{J_{ro}n_o}{{J_{rt}}^2}\tfrac{a}{b}\int_0^t \overline{U}_w(s)\tfrac{b}{(s+a)^2+b^2}d\tau + A\tfrac{\eta_b}{{J_{rt}}^2}\int_0^t \overline{U}_z(s)\tfrac{1}{s}d\tau + \\
& -A\tfrac{\eta_w}{{J_{rt}}^2}\int_0^t \overline{U}_z(s)\tfrac{s+a}{(s+a)^2+b^2}d\tau + A\tfrac{\eta_w}{{J_{rt}}^2}\tfrac{a}{b}\int_0^t \overline{U}_z(s)\tfrac{b}{(s+a)^2+b^2}d\tau \\
& + \tfrac{1}{J_{rt}b}\overline{U}_z(s)\tfrac{b}{(s+a)^2+b^2}
\end{aligned} \tag{20}$$

Finally, using the inverse Laplace transform and taking into account the relationships in (5) and (6), the dependencies describing the tilt and deflections angles of the gyroscope axis in space as a function of time were determined.

$$\begin{aligned}
\theta_w(t) = \; & -A\tfrac{J_{ro}n_o}{{J_{rt}}^2}\int_0^t U_z(\tau)\,d\tau + A\tfrac{J_{ro}n_o}{{J_{rt}}^2}\int_0^t U_z(\tau)e^{-a(t-\tau)}\cos(b(t-\tau))\,d\tau + \\
& -A\tfrac{J_{ro}n_o}{{J_{rt}}^2}\tfrac{a}{b}\int_0^t U_z(\tau)e^{-a(t-\tau)}\sin(b(t-\tau))\,d\tau + A\tfrac{\eta_z}{{J_{rt}}^2}\int_0^t U_w(\tau)\,d\tau + \\
& -A\tfrac{\eta_z}{{J_{rt}}^2}\int_0^t U_w(\tau)e^{-a(t-\tau)}\cos(b(t-\tau))\,d\tau \\
& +A\tfrac{\eta_z}{{J_{rt}}^2}\tfrac{a}{b}\int_0^t U_w(\tau)e^{-a(t-\tau)}\sin(b(t-\tau))\,d\tau \\
& + \tfrac{1}{J_{rt}b}\int_0^t U_w(\tau)e^{-a(t-\tau)}\sin(b(t-\tau))\,d\tau
\end{aligned} \tag{21}$$

$$\begin{aligned}\theta_z(t) = \; & A\tfrac{J_{ro}n_o}{J_{rt}{}^2}\int_0^t U_w(\tau)\,d\tau - A\tfrac{J_{ro}n_o}{J_{rt}{}^2}\int_0^t U_w(\tau)e^{-a(t-\tau)}\cos(b(t-\tau))\,d\tau \\ & + A\tfrac{J_{ro}n_o}{J_{rt}{}^2}\tfrac{a}{b}\int_0^t U_w(\tau)e^{-a(t-\tau)}\sin(b(t-\tau))\,d\tau + A\tfrac{\eta_w}{J_{rt}{}^2}\int_0^t U_z(\tau)\,d\tau + \\ & - A\tfrac{\eta_w}{J_{rt}{}^2}\int_0^t U_z(\tau)e^{-a(t-\tau)}\cos(b(t-\tau))\,d\tau \\ & + A\tfrac{\eta_w}{J_{rt}{}^2}\tfrac{a}{b}\int_0^t U_z(\tau)e^{-a(t-\tau)}\sin(b(t-\tau))\,d\tau \\ & + \tfrac{1}{J_{rt}b}\int_0^t U_z(\tau)e^{-a(t-\tau)}\sin(b(t-\tau))\,d\tau\end{aligned} \tag{22}$$

The analytical equations outlined unambiguously describe the inclinations and deviations of the gyroscope axis over time, allowing a series of analyses of the dynamics of the kinematic system to be under investigation.

3. Results and Discussion

Mechanical gyroscopes are used in various fields such as marine navigation, aviation, aerospace, and mechanical engineering. Their main advantage is reliability in extreme conditions, where electronic devices can be susceptible to electromagnetic interference or power failures. In marine navigation and aerospace, mechanical gyroscopes provide stable orientation without the need for constant access to external signals, which is crucial in the event of loss of communication or severe weather conditions.

Mechanical gyroscopes are often used in stabilization systems where precise motion control is required, such as for stabilizing cameras or rotating platforms. The design of the mechanical gyroscope mechanism allows for long-lasting operation without frequent calibration or maintenance, which can be important in industrial applications. Compared to electronic gyros, mechanical gyros also often have a higher resistance to external interference and extreme temperatures, making them more versatile in a variety of operating conditions.

Mechanical gyroscopes are characterized by a greater weight and size compared to their electronic counterparts, which can be important in applications where compact solutions are required. Despite this, mechanical gyros are still an indispensable technological component in many critical applications where reliability and resistance to extreme conditions are key.

The following are the results of a simulation study of the presented mathematical model for the motion of a gyroscope system with a rotating mass and Cardan suspension, subjected to external moments. This model was solved using two methods: with the derivation of an analytical solution and the use of numerical methods.

Numerical studies of the dynamics of the gyroscope described by Equations (5) and (6), subjected to the action of the control moments ((3) and (4)), have been carried out in the Matlab/Simulink R2021b environment, using the ode45, integration procedure, with a constant integration step of $dt = 0.00001$ s. The following gyro parameter values were taken into consideration:

$$J_{ro} = 0.0446\ \text{kgm}^2,\ J_{rt} = 0.0223\ \text{kgm}^2,\ n_o = 600\ \text{rad/s},\ \eta_w = \eta_z = 0.5\ \text{Nm/s}.$$

The graphs below show the obtained profiles of the tilt and deviation angles of the gyroscope axis for analytical and numerical solutions of the gyroscope motion equations for several cases of control moments acting on the gyroscope frame.

3.1. Case 1

Figures 2 and 3 show a comparison of the analytical and numerical solutions of the equations of motion of a gyroscope for control moments in the form of a rectangular impulse.

$$U_w = U_z = \begin{cases} 5 \ for \ t_1 < t \leq t_2 \\ 0 \ in \ other \ case \end{cases},$$

where: $t_1 = 1.5\,\mathrm{s}$, $t_2 = 3.0\,\mathrm{s}$.

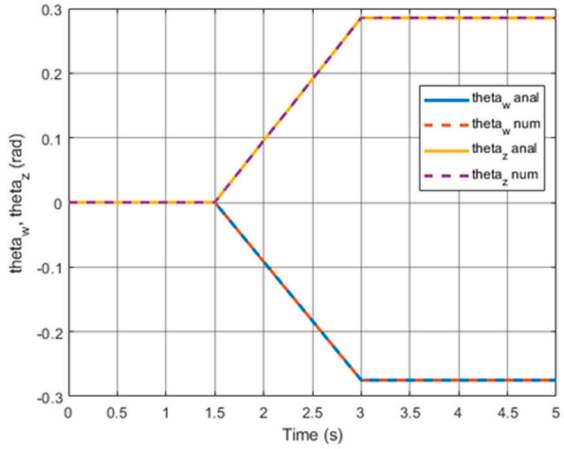

Figure 2. Angles of inclination and deviation of the gyroscope axis, obtained from the analytical (anal.) and numerical (num.) solutions, as a function of time.

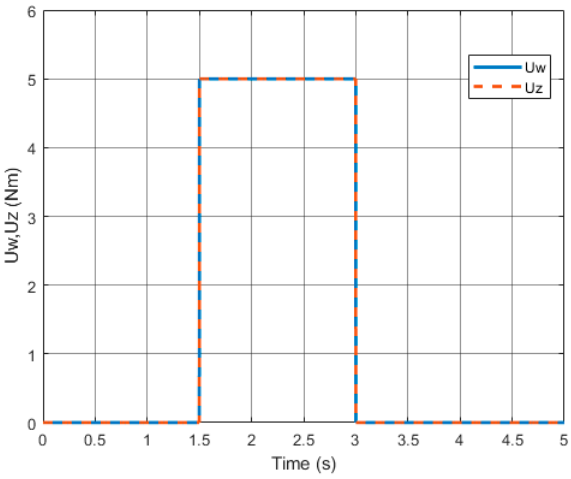

Figure 3. Control moments in function of time.

For control moments step-changing from 0 to a value of 5 Nm after time $t_1 = 1.5\,\mathrm{s}$ and axing 0 Nm again after time $t_2 = 3.0\,\mathrm{s}$, θ_w and θ_z angles vary linearly in the time interval t_1 to t_2, reaching values of -0.3 and 0.3 rad, respectively.

3.2. Case 2

Figures 4 and 5 show a comparison of the analytical and numerical solutions of the motion equations of a gyroscope for control moments in the form of a triangular impulse.

$$U_w = U_z = \begin{cases} \frac{U_0}{t_1 - t_0}(t - t_0) \ for \ t_0 < t \leq t_1 \\ \frac{U_0}{t_2 - t_1}(t_2 - t) \ for \ t_1 < t \leq t_2 \\ 0 \ in \ other \ case \end{cases}$$

where: $U_0 = 5.0\,\mathrm{N\,m}$, $t_0 = 1.0\,\mathrm{s}$, $t_1 = 3.0\,\mathrm{s}$, and $t_1 = 5.0\,\mathrm{s}$.

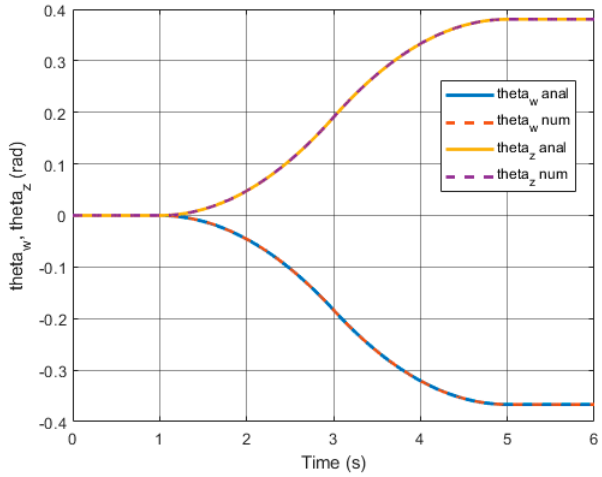

Figure 4. Angles of inclination and deviation of the gyroscope axis, obtained from the analytical (anal.) and numerical (num.) solutions, in function of time.

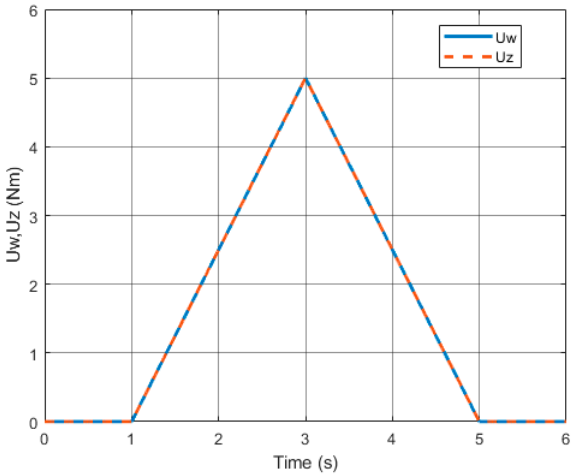

Figure 5. Control moments in function of time.

For *case 2*, the change of control moments is described by a spline function. The function increases linearly from t_0 to t_1 in the range from 0 to 5 Nm. After time t_1, the control moment decreases linearly to 0 for t_2. On the other hand, θ_w and θ_z angles change as shown in Figure 4 and reach a maximum value close to -0.4 and 0.4 rad, respectively, after time $t_2 = 5$ s.

3.3. Case 3

Figures 6 and 7 show a comparison of the analytical and numerical solutions of the motion equations of a gyroscope for control moments in the form of a Heaviside function.

$$U_w = U_z = U_0 \; Heaviside(t - t_0),$$

where $U_0 = 5.0$ Nm, $t_0 = 1.5$ s.

Case 3 used the Heaviside function as the control moments, that is, at time $t_0 = 1.5$ s there is a step increase in moments from 0 to 5 Nm. The θ_w and θ_z angles begin to increase linearly from the same instant of time t_0, as shown in Figure 6.

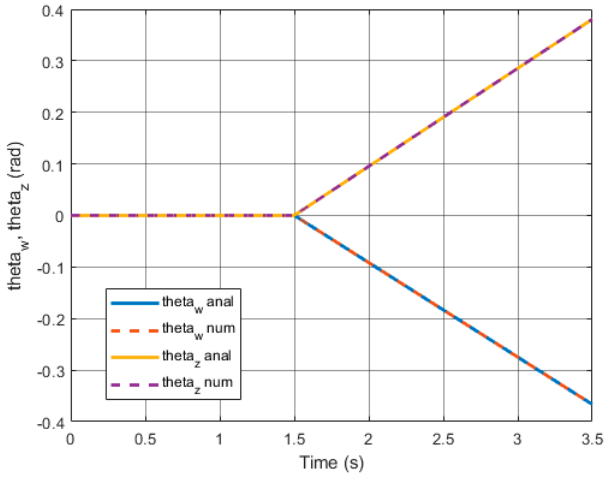

Figure 6. Angles of inclination and deviation of the gyroscope axis, obtained from the analytical (anal.) and numerical (num.) solutions, in function of time.

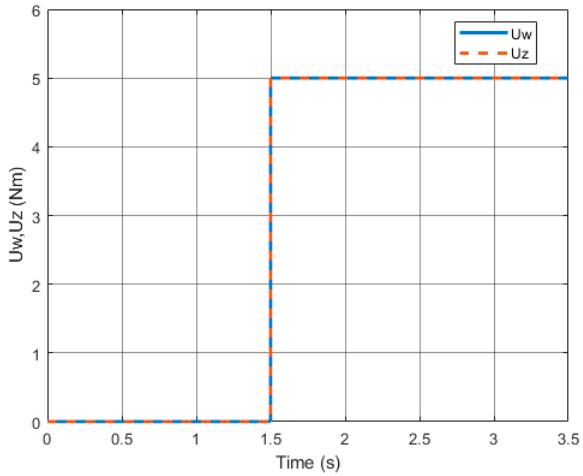

Figure 7. Control moments in function of time.

3.4. Case 4

Figures 8 and 9 show a comparison of the analytical and numerical solutions of the motion equations of a gyroscope for harmonic control moments, described as the following equation.

$$U_w = U_0 \ \sin(v\,t)$$

$$U_z = U_0 \ \cos(v\,t)$$

where: $U_0 = 5.0\,\mathrm{Nm}$, $v = 50\,\mathrm{rad/s}$.

For control moments described by trigonometric functions of given amplitude and frequency, θ_w and θ_z angles also have a waveform corresponding to the nature of these functions. The values of the angles change in the range $1.4827 \times 10^{-4} \div 0.00732\,\mathrm{rad}$ for θ_z and $-0.00352 \div 0.00366\,\mathrm{rad}$ for θ_w.

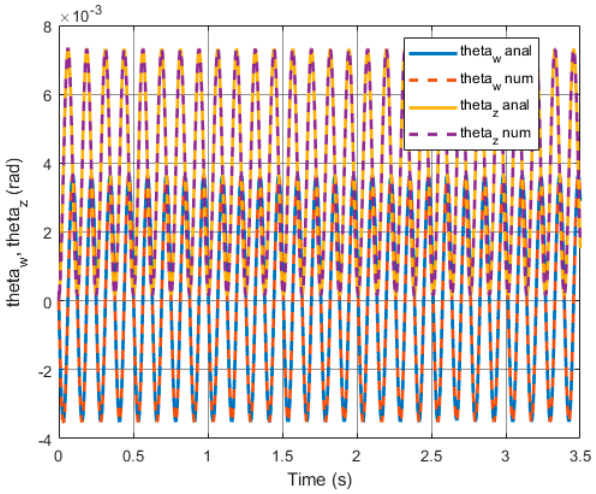

Figure 8. Angles of inclination and deviation of the gyroscope axis, obtained from the analytical (anal.) and numerical (num.) solutions, in function of time.

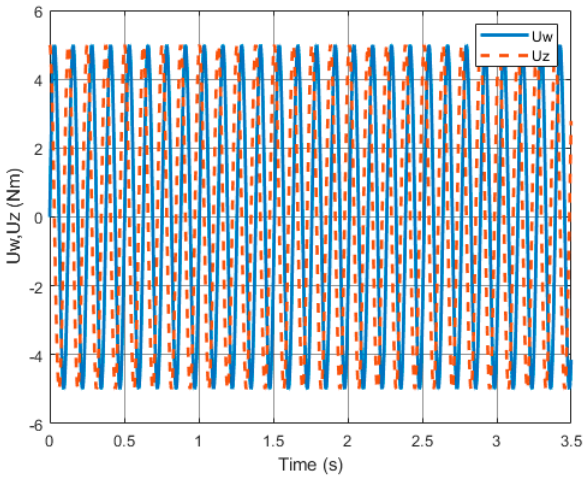

Figure 9. Control moments in function of time.

3.5. Case 5

Figures 10 and 11 show a comparison of the analytical and numerical solutions of the motion equations of a gyroscope for control moments, described as the following equation:

$$U_w = U_0 \left(1 + \frac{1}{1 + 10^{-3(t_0 - t)}}\right) \sin(v\,t),$$

$$U_z = U_0 \left(1 + \frac{1}{1 + 10^{-3(t_0 - t)}}\right) \cos(v\,t),$$

where: $U_0 = 5.0\,\mathrm{Nm}$, $v = 50\,\mathrm{rad/s}$, and $t_0 = 1.0\,\mathrm{s}$.

In this case, a smooth reduction in the control moment from 10 Nm to a reference value of 5 Nm was applied using the function described by the first term of the control moment relation. However, the use of such a function has a disadvantage related to a certain delay introduced into the control system.

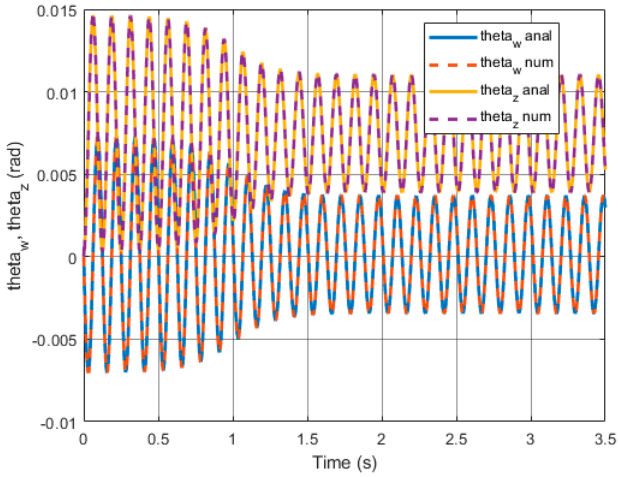

Figure 10. Angles of inclination and deviation of the gyroscope axis, obtained from the analytical (anal.) and numerical (num.) solutions, in function of time.

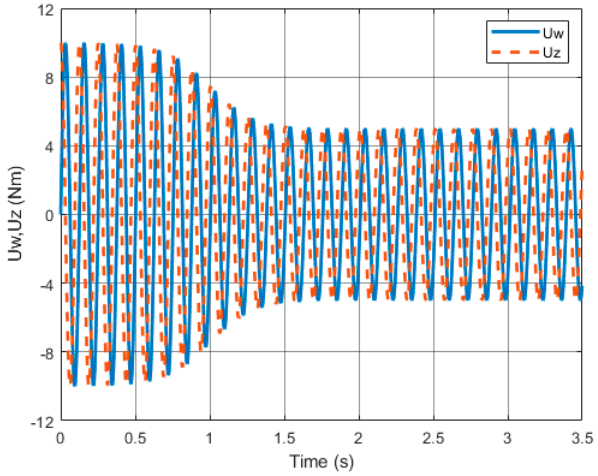

Figure 11. Control moments in function of time.

3.6. Case 6

Figures 12 and 13 show a comparison of the analytical and numerical solutions of the motion equations of a gyroscope for control moments, described as the following equation:

$$U_w = U_0 \left(\frac{1}{1 + 10^{3(t_0 - t)}} \right) \sin(v\,t),$$

$$U_z = U_0 \left(\frac{1}{1 + 10^{3(t_0 - t)}} \right) \cos(v\,t),$$

where: $U_0 = 5.0\,\mathrm{Nm}$, $v = 50\,\mathrm{rad/s}$, and $t_0 = 1.0\,\mathrm{s}$.

As can be seen in Figure 13, the control moments are trigonometric functions, where in the time interval from t = 0.5 to 1.5 s there is an increase in the amplitude of the control moments in the range of 0 to 5 Nm. The resulting values of θ_w and θ_z angles are from -3.5×10^{-3} to 3.5×10^{-3} rad.

In all cases, the results obtained are characterized by high convergence. To compare the results obtained, a certain evaluation criterion was introduced.

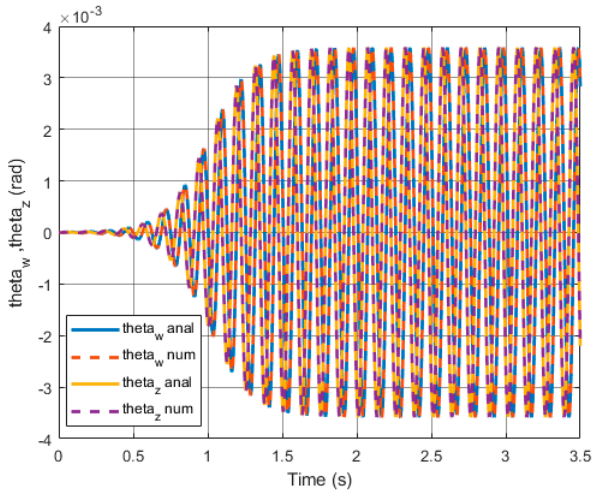

Figure 12. Angles of inclination and deviation of the gyroscope axis, obtained from the analytical (anal.) and numerical (num.) solutions, in function of time.

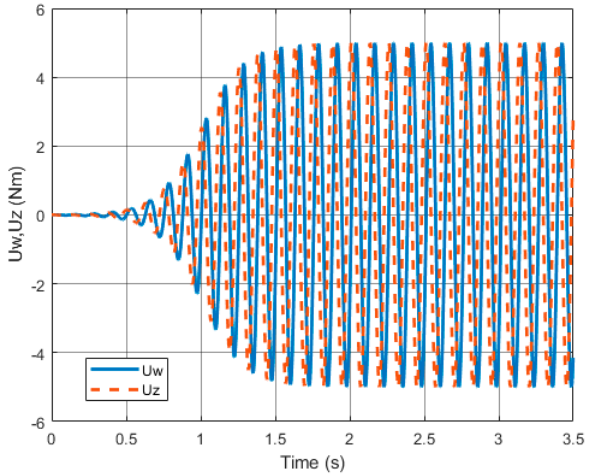

Figure 13. Control moments in function of time.

The following indicators were proposed for the comparative evaluation of the analytical and numerical solutions:

$$s\_\theta_w = \sum_{t=0}^{t_k} (\theta_{w\_num} - \theta_{w\_anal})^2 \tag{23}$$

$$s\_\theta_z = \sum_{t=0}^{t_k} (\theta_{z\_num} - \theta_{z\_anal})^2 \tag{24}$$

where:

s_θ_w—calculated sum of the error for the inclination angle of the gyroscope axis;
s_θ_z—calculated sum of the error for the deviation angle of the gyroscope axis;
num—numerical solution;
anal—analytical solution;
t_k—simulation end time.

Table 1 presents a summary of the comparative indicators designated according to the proposed criterion (23) and (24).

It is clear from the above graphs and comparative indicators that the analytical solutions (21) and (22) are in complete agreement with the numerical solutions, regardless of the form of the control moments acting on the gyroscopic frame. The correctness of the

analytical solutions determining the inclination and deviation angles of the gyroscope axis, as derived in Section 2, has been confirmed in this manner.

Table 1. Comparative indicators.

Cases	Indicator s_θ_w	Indicator s_θ_z
Case 1	2.6908×10^{-7}	2.6618×10^{-7}
Case 2	2.7420×10^{-7}	2.9534×10^{-7}
Case 3	1.0145×10^{-7}	9.7477×10^{-8}
Case 4	4.3220×10^{-8}	4.0442×10^{-8}
Case 5	1.3427×10^{-7}	1.2304×10^{-7}
Case 6	1.1802×10^{-8}	1.1900×10^{-8}

4. Conclusions

The main objective of this paper was to compare the results obtained from the analytical and numerical solutions to the system of equations describing the motion of a gyroscope suspended on a Cardan joint under the influence of control torque moments. The presented results of analytical and numerical solutions have been obtained for various forms of continuous and discontinuous control inputs of torque moments. Functions describing control torques have been adopted for exemplary excitations generated by the control system, using a combination of linear trigonometric, Gauss, Heaviside, and spline functions.

An analytical solution of the system of ordinary differential equations together with the initial conditions, using the Laplace transform and Green's function, has been presented. In a closed form, dependencies were obtained that describe changes over time in the angles of inclination and deviation of the gyroscope axis. The results were compared with those obtained using a conventional method, such as the fourth-order Runge–Kutta method, which is often used to solve ordinary differential equations.

The analysis of results has been conducted for six cases, involving various forms of control moments. Complete equality was obtained between analytical and numerical solutions as a result of the comparison. It has been established that the proposed analytical solutions are correct. In addition, they are versatile enough so that, regardless of the functions describing the control moments, particular relations for the angles of the gyroscope axis in space can be obtained quite easily.

In conclusion, the proposed analytical approach is precise and effective. It avoids the problems encountered in traditional numerical solutions, such as time discretization stability and interpolation errors.

Author Contributions: Conceptualization, I.K. and S.B.; methodology, I.K. and S.B.; software, I.K. and S.B.; validation, I.K.; formal analysis, I.K. and S.B.; investigation, I.K. and S.B.; resources, I.K. and S.B.; data curation, I.K.; writing—original draft preparation, I.K. and S.B.; writing—review and editing, I.K. and S.B.; visualization, I.K. and S.B.; supervision, I.K. and S.B. All authors have read and agreed to the published version of the manuscript.

Funding: This research received no external funding.

Data Availability Statement: The data presented in this study are available in this article.

Conflicts of Interest: The authors declare no conflicts of interest.

Appendix A

Solution of system of Equations (5) and (6), applying Laplace's transform (7)–(9) with the boundary conditions, we will receive the Equations (17) and (18).

We calculate from the system of Equations (17) and (18) values of $\overline{\theta}_w(s)$ and $\overline{\theta}_z(s)$.

$$\begin{array}{l} \frac{J_{ro}n_o}{J_{rt}} s\overline{\theta}_z(s) = \frac{1}{J_{rt}}\overline{U}_w(s) - s^2\overline{\theta}_w(s) - \frac{\eta_w}{J_{rt}} s\overline{\theta}_w(s) \\ \frac{J_{ro}n_o}{J_{rt}} s\overline{\theta}_w(s) = -\frac{1}{J_{rt}}\overline{U}_z(s) + s^2\overline{\theta}_z(s) + \frac{\eta_z}{J_{rt}} s\overline{\theta}_z(s) \end{array} \quad \text{(A1)}$$

$$\begin{array}{l}\overline{\theta}_z(s) = \frac{1}{J_{ro}n_o}\frac{1}{s}\overline{U}_w(s) - \frac{J_{rt}}{J_{ro}n_o}s\overline{\theta}_w(s) - \frac{\eta_w}{J_{ro}n_o}\overline{\theta}_w(s)\\ \overline{\theta}_w(s) = -\frac{1}{J_{ro}n_o}\frac{1}{s}\overline{U}_z(s) + \frac{J_{rt}}{J_{ro}n_o}s\overline{\theta}_z(s) + \frac{\eta_z}{J_{ro}n_o}\overline{\theta}_z(s)\end{array} \tag{A2}$$

We put the determined values back into the system of equations

$$\begin{array}{l}J_{rt}s^2\left(-\frac{1}{J_{ro}n_o}\frac{1}{s}\overline{U}_z(s) + \frac{J_{rt}}{J_{ro}n_o}s\overline{\theta}_z(s) + \frac{\eta_z}{J_{ro}n_o}\overline{\theta}_z(s)\right)+\\ +\eta_w s\left(-\frac{1}{J_{ro}n_o}\frac{1}{s}\overline{U}_z(s) + \frac{J_{rt}}{J_{ro}n_o}s\overline{\theta}_z(s) + \frac{\eta_z}{J_{ro}n_o}\overline{\theta}_z(s)\right) + J_{ro}n_o s\overline{\theta}_z(s) = \overline{U}_w(s)\\ J_{rt}s^2\left(\frac{1}{J_{ro}n_o}\frac{1}{s}\overline{U}_w(s) - \frac{J_{rt}}{J_{ro}n_o}s\overline{\theta}_w(s) - \frac{\eta_w}{J_{ro}n_o}\overline{\theta}_w(s)\right)+\\ +\eta_z s\left(\frac{1}{J_{ro}n_o}\frac{1}{s}\overline{U}_w(s) - \frac{J_{rt}}{J_{ro}n_o}s\overline{\theta}_w(s) - \frac{\eta_w}{J_{ro}n_o}\overline{\theta}_w(s)\right) - J_{ro}n_o s\overline{\theta}_w(s) = \overline{U}_z(s)\end{array} \tag{A3}$$

After performing algebraic calculations, the result was:

$$\begin{array}{l}\left(s^2 + \left(\frac{\eta_z+\eta_w}{J_{rt}}\right)s + \frac{\eta_z\eta_w+(J_{ro}n_o)^2}{{J_{rt}}^2}\right)\overline{\theta}_z(s) = \frac{J_{ro}n_o}{{J_{rt}}^2}\frac{1}{s}\overline{U}_w(s) + \frac{\eta_w}{{J_{rt}}^2}\frac{1}{s}\overline{U}_z(s) + \frac{1}{J_{rt}}\overline{U}_z(s)\\ \left(s^2 + \left(\frac{\eta_z+\eta_w}{J_{rt}}\right)s + \frac{\eta_z\eta_w+(J_{ro}n_o)^2}{{J_{rt}}^2}\right)\overline{\theta}_w(s) = \frac{\eta_z}{{J_{rt}}^2}\frac{1}{s}\overline{U}_w(s) - \frac{J_{ro}n_o}{{J_{rt}}^2}\frac{1}{s}\overline{U}_z(s) + \frac{1}{J_{rt}}\overline{U}_w(s)\end{array} \tag{A4}$$

Once the substitutions are in place:

$$s^2 + \left(\frac{\eta_z+\eta_w}{J_{rt}}\right)s + \frac{\eta_z\eta_w+(J_{ro}n_o)^2}{{J_{rt}}^2} = \left(s + \frac{1}{2}\left(\frac{\eta_z+\eta_w}{J_{rt}}\right)\right)^2 + \left(\frac{\eta_z\eta_w+(J_{ro}n_o)^2}{{J_{rt}}^2}\right) - \frac{1}{4}\left(\frac{\eta_z+\eta_w}{J_{rt}}\right)^2 \tag{A5}$$

$$a = \frac{1}{2}\left(\frac{\eta_z+\eta_w}{J_{rt}}\right) \tag{A6}$$

$$b^2 = \left(\frac{\eta_z\eta_w+(J_{ro}n_o)^2}{{J_{rt}}^2}\right) - \frac{1}{4}\left(\frac{\eta_z+\eta_w}{J_{rt}}\right)^2 > 0 \tag{A7}$$

The Equation (A5) can be written:

$$s^2 + \left(\frac{\eta_z+\eta_w}{J_{rt}}\right)s + \left(\frac{\eta_z\eta_w+(J_{ro}n_o)^2}{{J_{rt}}^2}\right) = (s+a)^2 + b^2 \tag{A8}$$

Obtained:

$$\begin{array}{l}\left((s+a)^2 + b^2\right)\overline{\theta}_z(s) = \frac{J_{ro}n_o}{{J_{rt}}^2}\frac{1}{s}\overline{U}_w(s) + \frac{\eta_w}{{J_{rt}}^2}\frac{1}{s}\overline{U}_z(s) + \frac{1}{J_{rt}}\overline{U}_z(s)\\ \left((s+a)^2 + b^2\right)\overline{\theta}_w(s) = \frac{\eta_z}{{J_{rt}}^2}\frac{1}{s}\overline{U}_w(s) - \frac{J_{ro}n_o}{{J_{rt}}^2}\frac{1}{s}\overline{U}_z(s) + \frac{1}{J_{rt}}\overline{U}_w(s)\end{array} \tag{A9}$$

Transforming Equation (A9) yielded the following:

$$\begin{array}{l}\overline{\theta}_z(s) = \frac{J_{ro}n_o}{{J_{rt}}^2}\frac{\overline{U}_w(s)}{s\left((s+a)^2+b^2\right)} + \frac{\eta_w}{{J_{rt}}^2}\frac{\overline{U}_z(s)}{s\left((s+a)^2+b^2\right)} + \frac{1}{J_{rt}}\frac{\overline{U}_z(s)}{\left((s+a)^2+b^2\right)}\\ \overline{\theta}_w(s) = \frac{\eta_z}{{J_{rt}}^2}\frac{\overline{U}_w(s)}{s\left((s+a)^2+b^2\right)} - \frac{J_{ro}n_o}{{J_{rt}}^2}\frac{\overline{U}_z(s)}{s\left((s+a)^2+b^2\right)} + \frac{1}{J_{rt}}\frac{\overline{U}_w(s)}{\left((s+a)^2+b^2\right)}\end{array} \tag{A10}$$

$$\begin{array}{l}\frac{1}{s\left((s+a)^2+b^2\right)} \equiv \frac{A}{s} + \frac{Bs+C}{(s+a)^2+b^2} = \frac{A\left((s+a)^2+b^2\right)}{s\left((s+a)^2+b^2\right)} + \frac{Bs^2+Cs}{s\left((s+a)^2+b^2\right)} =\\ \frac{A(s+a)^2+Ab^2}{s\left((s+a)^2+b^2\right)} + \frac{Bs^2+Cs}{s\left((s+a)^2+b^2\right)} = \frac{A\left(s^2+2a+a^2\right)+Ab^2+Bs^2+Cs}{s\left((s+a)^2+b^2\right)} = \frac{As^2+A2a+Aa^2+Ab^2+Bs^2+Cs}{s\left((s+a)^2+b^2\right)}\end{array} \tag{A11}$$

By decomposing the successive components of the system of Equation (A10) into simple fractions according to the relation (A11), we obtained:

$$\begin{array}{l}\overline{\theta}_z(s) = \frac{J_{ro}n_o}{{J_{rt}}^2}\overline{U}_w(s)\left(A\frac{1}{s} - A\frac{s+a-a}{(s+a)^2+b^2}\right) + \frac{\eta_w}{{J_{rt}}^2}\overline{U}_z(s)\left(A\frac{1}{s} - A\frac{s+a-a}{(s+a)^2+b^2}\right) + \frac{1}{J_{rt}b}\overline{U}_z(s)\frac{b}{\left((s+a)^2+b^2\right)}\\ \overline{\theta}_w(s) = -\frac{J_{ro}n_o}{{J_{rt}}^2}\overline{U}_z(s)\left(A\frac{1}{s} - A\frac{s+a-a}{(s+a)^2+b^2}\right) + \frac{\eta_z}{{J_{rt}}^2}\overline{U}_w(s)\left(A\frac{1}{s} - A\frac{s+a-a}{(s+a)^2+b^2}\right) + \frac{1}{J_{rt}b}\overline{U}_w(s)\frac{b}{\left((s+a)^2+b^2\right)}\end{array} \tag{A12}$$

The final form of equations was determined by (19) and (20). The final step is to apply the inverse transform.

References

1. Amer, W.S. The dynamical motion of a gyroscope subjected to applied moments. *Results Phys.* **2019**, *12*, 1429–1435. [CrossRef]
2. Scarborough, J.B. *The Gyroscope Theory and Applications*; Creative Media Partners, LLC: New York, NY, USA, 2022; ISBN 9781015443938.
3. Cordeiro, F.J.B. *Gyroscope*; Nabu Press: New York, NY, USA, 2010; ISBN 1176280007.
4. Chen, H.-K. Chaos and chaos synchronization of a symmetric gyro with linear-plus-cubic damping. *J. Sound Vib.* **2002**, *255*, 719–740. [CrossRef]
5. Van Dooren, R. Comments on "Chaos and chaos synchronization of a symmetric gyro with linear-plus-cubic damping". *J. Sound Vib.* **2003**, *268*, 632–634. [CrossRef]
6. Ge, Z.-M.; Lee, J.-K. Chaos synchronization and parameter identification for gyroscope system. *Appl. Math. Comput.* **2005**, *163*, 667–682. [CrossRef]
7. Lei, Y.; Xu, W.; Zheng, H. Synchronization of two chaotic nonlinear gyros using active control. *Phys. Lett. A* **2005**, *343*, 153–158. [CrossRef]
8. Salarieh, H. Comment on: "Synchronization of two chaotic nonlinear gyros using active control" [Phys. Lett. A 343 (2005) 153]. *Phys. Lett. A* **2008**, *372*, 2539–2540. [CrossRef]
9. Chen, H.-K.; Ge, Z.-M. Bifurcations and chaos of a two-degree-of-freedom dissipative gyroscope. *Chaos Solitons Fractals* **2005**, *24*, 125–136. [CrossRef]
10. Yau, H.-T. Nonlinear rule-based controller for chaos synchronization of two gyros with linear-plus-cubic damping. *Chaos Solitons Fractals* **2007**, *34*, 1357–1365. [CrossRef]
11. Sargolzaei, M.; Yaghoobi, M.; Yazdi, R.A.G. Modeling and synchronization of chaotic gyroscopes using TS fuzzy approach. *Adv. Electron. Electr. Eng.* **2013**, *3*, 339–346.
12. Yan, J.-J.; Hung, M.-L.; Lin, J.-S.; Liao, T.-L. Controlling chaos of a chaotic nonlinear gyro using variable structure control. *Mech. Syst. Signal Process.* **2007**, *21*, 2515–2522. [CrossRef]
13. Yau, H.-T. Chaos synchronization of two uncertain chaotic nonlinear gyros using fuzzy sliding mode control. *Mech. Syst. Signal Process.* **2008**, *22*, 408–418. [CrossRef]
14. Yau, H.-T. Generalized projective chaos synchronization of gyroscope systems subjected to dead-zone nonlinear inputs. *Phys. Lett. A* **2008**, *372*, 2380–2385. [CrossRef]
15. Roopaei, M.; Zolghadri Jahromi, M.; John, R.; Lin, T.-C. Unknown nonlinear chaotic gyros synchronization using adaptive fuzzy sliding mode control with unknown dead-zone input. *Commun. Nonlinear Sci. Numer. Simul.* **2010**, *15*, 2536–2545. [CrossRef]
16. Wang, C.-C.; Yau, H.-T. Nonlinear dynamic analysis and sliding mode control for a gyroscope system. *Nonlinear Dyn.* **2011**, *66*, 53–65. [CrossRef]
17. Chen, S.-C.; Kuo, C.-L.; Lin, C.-H.; Hsu, C.-H.; Tsui, C.-K. Applications of Fuzzy Sliding Mode Control for a Gyroscope System. *Abstr. Appl. Anal.* **2013**, *2013*, 931285. [CrossRef]
18. Usubamatov, R. Analysis of Motions for Gyroscope with One Side Support Article Information. *Sch. J. Appl. Sci. Res.* **2018**, *1*, 5–13.
19. Awrejcewicz, J.; Koruba, Z. *Classical Mechanics*; Springer: New York, NY, USA, 2012; ISBN 978-1-4614-3977-6.
20. Krzysztofik, I.; Takosoglu, J.; Koruba, Z. Selected methods of control of the scanning and tracking gyroscope system mounted on a combat vehicle. *Annu. Rev. Control* **2017**, *44*, 173–182. [CrossRef]
21. He, H.; Xie, X.; Wang, W. Vibration Control of Tower Structure with Multiple Cardan Gyroscopes. *Shock Vib.* **2017**, *2017*, 3548360. [CrossRef]
22. Lungu, M. Control of double gimbal control moment gyro systems using the backstepping control method and a nonlinear disturbance observer. *Acta Astronaut.* **2021**, *180*, 639–649. [CrossRef]
23. Kojima, H.; Nakamura, R.; Keshtkar, S. Model predictive steering control law for double gimbal scissored-pair control moment gyros. *Acta Astronaut.* **2021**, *183*, 273–285. [CrossRef]
24. Papakonstantinou, C.; Lappas, V.; Kostopoulos, V. A Gimballed Control Moment Gyroscope Cluster Design for Spacecraft Attitude Control. *Aerospace* **2021**, *8*, 273. [CrossRef]